PHYSICAL REVIEW B **88**, 064421 (2013)

Field-induced phase transitions in the helimagnet $Ba_2CuGe_2O_7$

J. Chovan,[1,*] M. Marder,[2,†] and N. Papanicolaou[3,‡]
[1]*Department of Physics, Matej Bel University, Banská Bystrica, Slovakia*
[2]*Center for Nonlinear Dynamics and Department of Physics, The University of Texas at Austin, Austin, Texas 78712, USA*
[3]*Department of Physics and Institute of Plasma Physics, University of Crete, Heraklion, Greece*

(Received 24 November 2012; revised manuscript received 29 June 2013; published 26 August 2013)

We present a theoretical study of the two-dimensional spiral antiferromagnet $Ba_2CuGe_2O_7$ in the presence of an external magnetic field. We employ a suitable nonlinear σ model to calculate the $T = 0$ phase diagram and the associated low-energy spin dynamics for arbitrary canted magnetic fields, in general agreement with experiment. In particular, when the field is applied parallel to the c axis, a previously anticipated Dzyaloshinskii-type incommensurate-to-commensurate phase transition is actually mediated by an intermediate phase, in agreement with our earlier theoretical prediction confirmed by the recent observation of the so-called double-k structure. The sudden $\pi/2$ rotations of the magnetic structures observed in experiment are accounted for by a weakly broken $U(1)$ symmetry of our model. Finally, our analysis suggests a nonzero weak-ferromagnetic component in the underlying Dzyaloshinskii-Moriya anisotropy, which is important for quantitative agreement with experiment.

DOI: 10.1103/PhysRevB.88.064421 PACS number(s): 75.30.Ds, 75.30.Gw, 75.30.Kz

I. INTRODUCTION

The presence of Dzyaloshinskii-Moriya (DM) anisotropy[1,2] in low-symmetry magnetic crystals typically leads to weak ferromagnetism, as a result of slight spin canting in an otherwise antiferromagnetic (AF) ground state. Another possibility is the occurrence of helimagnetism whereby spins are arrayed in a helical or spiral structure whose period (pitch) extends over several decades of unit cells. These structures have intensively been studied lately, and the interest stems from a number of factors. Some DM helimagnets display appealing magnetoelectric or multiferroic properties.[3–5] This enables the control of unusual magnetic states by electric fields and vice versa, and makes these materials attractive for spintronics applications. Another major factor is that, in addition to one-dimensional (1D) spin spirals, the *ground states* can form a vortex (skyrmion) lattice, as advocated by Bogdanov *et al.*[6–8] in a number of related models. Recently, skyrmion-lattice ground states were observed experimentally in several magnetic systems.[4,9–11] Nontrivial types of localized *nonlinear excitations* (domain walls) in DM helimagnets have also been discussed in recent theoretical works.[12–14]

$Ba_2CuGe_2O_7$ is an example of a helimagnet well suited for experimental investigation thanks to a fortunate combination of physical properties. It is an insulator whose magnetic properties can be understood in terms of localized $s = \frac{1}{2}$ spins carried by the Cu^{2+} ions. The scale of energy set by an exchange constant $J \sim 1$ meV is very convenient for neutron scattering experiments. Because of the low tetragonal symmetry (space group $P\bar{4}2_1m$), the corresponding Heisenberg Hamiltonian involves an interesting combination of antisymmetric (DM) as well as symmetric exchange anisotropies which lead to a rich phase diagram. In particular, the strength of anisotropy is such that magnetic phase transitions take place at critical fields that are well within experimental reach.

A series of experiments in the late 1990s (Refs. 15–19) revealed the existence of a Dzyaloshinskii-type[20] incommensurate-to-commensurate (IC) phase transition when the strength of an external field applied along the c axis exceeds a critical value $H_c \sim 2$ T. For $H < H_c$, the ground state is an incommensurate spiral whose period $L = L(H)$ grows to infinity in the limit $H \to H_c$. For $H > H_c$, the ground state was thought to become a commensurate antiferromagnet, a *spin-flop* state. We note that the Dzyaloshinskii-type transition is similar to the cholesteric-nematic phase transition induced by an external magnetic field in chiral liquid crystals.[21–23] But, the IC transition observed in $Ba_2CuGe_2O_7$ was the first clean realization of the Dzyaloshinskii scenario in its original context, and as such still remains very rare.

We carried out a detailed theoretical investigation[24–26] inspired by the earlier experimental work[15–19] and predicted that the IC phase transition does not occur immediately; instead, between the incommensurate and commensurate phases occurs a separate *intermediate phase*. In short, there exist two critical fields H_{c1} and H_{c2} such that $H_{c1} < H_c < H_{c2}$ where $H_c \sim 2$ T is the critical field for the presumed Dzyaloshinskii-type phase transition. For $H < H_{c1} \sim 1.7$ T, the ground state is a flat spiral (cycloid) that propagates along the x axis while the staggered magnetization rotates in the xz plane. For $H > H_{c1}$, the cycloid transforms into a nonflat spiral where all three components of the staggered magnetization are different from zero. Such a state may concisely be described as an antiferromagnetic conical spiral that propagates along the x axis while it nutates around the y axis. Above $H_{c2} \sim 2.9$ T, the spiral becomes a conventional commensurate antiferromagnet. This state is a commensurate antiferromagnetic spin-flop state which is the ground state for all $H > H_{c2}$. Therefore, the Dzyaloshinskii field H_c is not a true critical field, and the corresponding IC phase transition is actually mediated by an additional phase in the region $H_{c1} < H < H_{c2}$.

This prediction[24] remained unexplored for almost a decade. Additional experimental work on $Ba_2CuGe_2O_7$ has revealed its remarkable magnetoelectric properties and demonstrated the electrical switching of magnetic propagation vector and the control of electric polarization by magnetic fields.[3] However, a new series of experiments has now confirmed the occurrence of an intermediate phase in the form of an antiferromagnetic conical spiral which has been called a *double-k structure* by the experimental discoverers. This state occurs as predicted when an external magnetic field is applied almost perfectly parallel to the c axis,[28] while further experiments have also explored the phase diagram in the presence of an arbitrary canted magnetic field.[29] It was not immediately evident to the experimentalists that they had found what we predicted. Our current task is to confirm that the recently observed double-k structure is indeed the intermediate phase predicted in Ref. 24 and further to calculate the phase diagram in arbitrary canted magnetic fields so as to complete the connection with the latest experiments.

In Sec. II, we describe the discrete spin Hamiltonian and its continuum approximation in the form of a nonlinear σ model. In Sec. III, the ground-state properties and the associated low-energy dynamics will be calculated from the nonlinear σ model for a magnetic field of varying strength and direction. Hence, in Sec. III A the field is restricted to point along the c (or z) axis and its strength is varied through the IC transition. We recover then results of Ref. 24 and further discuss the nature and stability of the intermediate phase. An explicit calculation of the low-energy magnon spectrum throughout the intermediate phase, and hence the opportunity for comparison with future experiments, is relegated to Appendix A. In Sec. III B, we study the case of a field applied in a direction perpendicular to the c axis. We thus recover an experimentally observed bisection rule and further illuminate the role of the out-of-plane DM anisotropy d_z. The case of a magnetic field applied in an arbitrary direction (canted magnetic field) is analyzed in Sec. III C where we present a theoretical prediction for the $T = 0$ phase diagram, in fair agreement with recent experiments. Local stability of the spin-flop phase in the presence of arbitrary canted fields is shortly discussed in Appendix B. Our main conclusions are summarized in Sec. IV.

II. NONLINEAR σ MODEL

In the method of calculation we closely follow the work of Ref. 24. $Ba_2CuGe_2O_7$ is a layered compound where the Cu atoms with spin $s = \frac{1}{2}$ form a perfect square lattice within each layer with natural axes x and y and lattice constant $l = 5.986$ Å. We note that the axes x, y differ from the conventional crystal axes a, b by a 45° azimuthal rotation. The major spin interaction between in-plane neighbors is antiferromagnetic, while the interaction between out-of-plane neighbors is ferromagnetic and weak. Therefore, the interlayer coupling is ignored in the following discussion which concentrates on the two-dimensional dynamics within each layer.

The two-dimensional (2D) spin Hamiltonian is of the general form

$$W = \sum_{\langle kl\rangle}[J_{kl}(\mathbf{S}_k\cdot\mathbf{S}_l) + \mathbf{D}_{kl}\cdot(\mathbf{S}_k\times\mathbf{S}_l)] + \frac{1}{2}\sum_{\langle kl\rangle}\sum_{i,j}G^{ij}_{kl}\left(S^i_kS^j_l + S^j_kS^i_l\right) - \sum_l(g\mu_B\mathbf{H}\cdot\mathbf{S}_l), \tag{1}$$

where $\mathbf{S}_k$ is the spin localized at site k, which satisfies the classical constraint $\mathbf{S}_k^2 = s^2$. The first and the second terms in Eq. (1) describe the isotropic exchange interaction and antisymmetric DM anisotropy over in-plane bonds denoted by $\langle kl\rangle$. The third term contains all symmetric exchange anisotropies, and the indices i and j are summed over the three three values corresponding to the Cartesian components of the spin vectors along the axes x, y, and z. Single-ion anisotropy is not present in this spin $s = \frac{1}{2}$ system. Finally, the last term describes the usual Zeeman interaction with an external field $\mathbf{H}$.

The form of the interaction parameters is significantly restricted by the crystal symmetry (space group $P\bar{4}2_1m$). It is safe to consider only nearest-neighbor (NN) in-plane bonds and neglect interactions between next-nearest neighbors.[24–26] Symmetry requires that the exchange constant $J = J_{kl}$ is the same for all NN in-plane bonds, whereas the constant vectors $\mathbf{D}_{kl}$ which account for pure DM anisotropy are of the form

$$\begin{aligned}\mathbf{D}_{kl} &= (0, D_\perp, \pm D_z)\ \text{ for bonds along }\ x,\\ \mathbf{D}_{kl} &= (D_\perp, 0, \pm D_z)\ \text{ for bonds along }\ y,\end{aligned} \tag{2}$$

where $D_\perp$ and $\pm D_z$ are two independent scalar constants. It should be noted that the z component of the DM vectors alternates in sign on opposite bonds, a feature that could lead to weak ferromagnetism. No such alternation occurs for the in-plane components of the DM vectors which are responsible for the observed spiral magnetic order or helimagnetism.

The symmetric exchange anisotropy will be restricted to the special Kaplan, Shekhtman, Entin-Wohlman, Aharony (KSEA) limit[30] throughout this paper. In this limit, the (traceless) symmetric tensor G^{ij}_{kl} is expressed entirely in terms of the corresponding DM vector $\mathbf{D}_{kl}$:

$$G^{ij}_{kl} = \frac{D^i_{kl}D^j_{kl}}{2J_{kl}} - \frac{|\mathbf{D}_{kl}|^2}{6J_{kl}}\delta_{ij}, \tag{3}$$

where δ_{ij} is the Kronecker delta. The KSEA limit has been shown to explain quantitatively a large set of experimental data,[17] including some finer issues such as the lattice pinning of helical magnetic domains,[27] and will be adopted here without further questioning. The Hamiltonian of Eq. (1) is still consistent with the underlying space group $P\bar{4}2_1m$ but is not the most general Hamiltonian allowed by symmetry.[24,26] To our knowledge, $Ba_2CuGe_2O_7$ is the only known pure KSEA system. In this respect, we mention that the layered antiferromagnet $K_2V_3O_8$ is not described by the KSEA anisotropy, as incorrectly stated in Ref. 31, because the observed easy-axis anisotropy is impossible to occur in the KSEA limit.[26]

The discrete Hamiltonian of Eq. (1) could be, in principle, analyzed by standard spin-wave techniques but such a task is technically complicated. The ground state and low-energy dynamics can be calculated from a simpler continuum field theory, which is a reasonable approximation because the period of the observed magnetic spiral is sufficiently long, about 37 lattice constants at zero field. We omit technical details but stress the important steps of the continuum approximation.

The major spin interaction is antiferromagnetic ($J = 0.96$ meV) and sets the energy scale of the system. We therefore divide a complete magnetic lattice into two sublattices A and B and then rewrite the Landau-Lifshitz equation as a system of two coupled equations for the sublattice spins $\mathbf{A}$ and $\mathbf{B}$. However, a more transparent formulation is obtained in terms of new variables, the magnetization $\mathbf{m} = (\mathbf{A} + \mathbf{B})/2s$ and the staggered magnetization $\mathbf{n} = (\mathbf{A} - \mathbf{B})/2s$, which satisfy the classical constraints $\mathbf{m}\cdot\mathbf{n}=0$ and $\mathbf{m}^2+\mathbf{n}^2=1$. The basis for the derivation of an effective field theory is the fact that all anisotropies and the applied field $D_\perp$, D_z, $g\mu_B H/s$ are significantly smaller than the exchange constant J. Consequently, $|\mathbf{m}|$ is also much smaller than $|\mathbf{n}|$, and both $\mathbf{m}$, $\mathbf{n}$ vary appreciably only over distances of many lattice spacings.

To ascertain the relative significance of the various terms that arise during a consistent low-energy reduction, one may employ a dimensionless scale ε defined from, say, $\varepsilon = D_\perp/J$. We further introduce rescaled (dimensionless) anisotropy $d_z=\sqrt{2}D_z/\varepsilon J$ and magnetic field $\mathbf{h}=g\mu_B\mathbf{H}/(2\sqrt{2}s\varepsilon J)$. Note that the unit of field ($h=1$) corresponds to $2\sqrt{2}s\varepsilon J/g\mu_B = 1.68$ T, where we use the values $s=\frac{1}{2}$, $g=2.474$, $J=0.96$ meV, and $\varepsilon=0.1774$ thought to be appropriate for the description of $Ba_2CuGe_2O_7$. Similarly, we introduce rationalized spatial coordinates x, y, and time t, and complete our choice with the statement that frequency is measured in units of $\hbar\omega = 2\sqrt{2}s\varepsilon J = 0.24$ meV, and distance in units of $l/\varepsilon = 33.75$ Å, where l is the lattice constant of the square lattice formed by the Cu atoms.

The continuum approximation is then obtained by a systematic formal expansion of Landau-Lifshitz equation in powers of ε, where both $\mathbf{m}$, $\mathbf{n}$ are considered as continuous functions of the (dimensionless) in-plane spatial coordinates x, y. The magnetization $\mathbf{m}$ is treated as a quantity of order ε, whereas the staggered magnetization $\mathbf{n}$ and the rescaled variables are assumed to be of order of unity. Then, to leading order, the classical constraints reduce to $\mathbf{m}\cdot\mathbf{n}=0$ and $\mathbf{n}^2=1$. Finally, the $T=0$ low-energy dynamics is expressed entirely in terms of the staggered magnetization $\mathbf{n}$, and is calculated from a nonlinear σ model with Lagrangian density $\mathcal{L}$:

$$\begin{aligned}\mathcal{L} &= \mathcal{L}_0 - V; \quad \mathcal{L}_0 = \tfrac{1}{2}\partial_0\mathbf{n}\cdot\partial_0\mathbf{n} + \mathbf{h}\cdot\mathbf{n}\times\partial_0\mathbf{n};\\ V &= \tfrac{1}{2}(\partial_1\mathbf{n}-\mathbf{e}_2\times\mathbf{n})^2 + \tfrac{1}{2}(\partial_2\mathbf{n}-\mathbf{e}_1\times\mathbf{n})^2\\ &\quad + \tfrac{1}{2}(\mathbf{n}\cdot\mathbf{h})^2 + d_z(\mathbf{h}\times\mathbf{e}_3)\cdot\mathbf{n}.\end{aligned} \tag{4}$$

Here $\mathbf{e}_1$, $\mathbf{e}_2$, and $\mathbf{e}_3$ are unit vectors along the x, y, and z axes, whereas derivatives are described by $\partial_1=\partial/\partial x$, $\partial_2=\partial/\partial y$, and $\partial_0=\partial/\partial t$. The applied magnetic field $\mathbf{h}=h_1\mathbf{e}_1+h_2\mathbf{e}_2+h_3\mathbf{e}_3$ may point in any arbitrary direction. We emphasize that the staggered magnetization $\mathbf{n}=n_1\mathbf{e}_1+n_2\mathbf{e}_2+n_3\mathbf{e}_3$ is a *unit-vector field* ($\mathbf{n}^2=1$) that depends upon the in-plane spatial coordinates x and y as well as the time variable t: $\mathbf{n}=\mathbf{n}(x,y,t)$. The in-plane component of the DM anisotropy $D_\perp$ has been completely suppressed in Eq. (4) through the definitions of rationalized units.

It should be noted that the special KSEA limit adopted here is equivalent to setting $\kappa=0$ in the Lagrangian of Ref. 24. Otherwise, Eq. (4) gives the most general Lagrangian compatible with symmetry, expressed in fully rationalized units. Rationalized units greatly simplify the analysis of Eq. (4) and will be employed throughout our theoretical development in the remainder of the paper. However, the critical or otherwise significant values of the field will occasionally be quoted also in physical units, in order to facilitate the orientation of the reader and comparison with experiment. Essentially for the same reason we use physical units in all figures directly relevant to experiment.[28,29]

III. $T = 0$ PHASE DIAGRAM

A. Field parallel to *c*

We begin by specializing to the case where the magnetic field is applied strictly along the c axis: $\mathbf{h}=h\mathbf{e}_3$. Then, the potential V of Eq. (4) reduces to

$$\begin{aligned}V &= \tfrac{1}{2}\left[(\partial_1\mathbf{n})^2+(\partial_2\mathbf{n})^2+(1+h^2)n_3^2+1\right]\\ &\quad -[(\partial_1 n_1-\partial_2 n_2)n_3-(n_1\partial_1-n_2\partial_2)n_3]\end{aligned} \tag{5}$$

and is symmetric under the $U(1)$ transformation

$$x+iy\rightarrow(x+iy)\,e^{i\psi}, \quad n_1+in_2\rightarrow(n_1+in_2)\,e^{-i\psi}, \tag{6}$$

which is somewhat unusual in that an azimuthal rotation of spatial coordinates x and y by an angle ψ is followed by a corresponding rotation of the staggered magnetization by an angle $-\psi$.

The ground state is obtained by finding energy-minimizing solutions $\mathbf{n}$ of the static energy functional

$$W=\int dx\,dy\,V. \tag{7}$$

In order to enforce the constraint that the staggered magnetization be of unit length, we adopt a parametrization

$$\mathbf{n}=\sin\Phi\sin\Theta\,\mathbf{e}_1+\cos\Theta\,\mathbf{e}_2+\cos\Phi\sin\Theta\,\mathbf{e}_3, \tag{8}$$

which differs from more standard parametrizations by a circular permutation, but turns out to yield slightly more compact expressions later on.

Our first task is to find solutions $\Theta=\Theta(x,y)$, $\Phi=\Phi(x,y)$ that minimize W. The minimum of energy is sought after in the form of the one-dimensional (1D) ansatz

$$\Theta(x,y)=\theta(x), \quad \Phi(x,y)=\phi(x), \tag{9}$$

which assumes that the staggered magnetization depends only on the spatial coordinate x. In view of the $U(1)$ symmetry in Eq. (6), any solution we find of this type automatically produces a family of additional solutions of the same energy rotated by angle ψ. Varying W then yields

$$\begin{aligned}\partial_1^2\phi &= -\frac{(2\,\partial_1\phi-2)\cos\theta\,\partial_1\theta+\gamma^2\cos\phi\,\sin\phi\,\sin\theta}{\sin\theta},\\ \partial_1^2\theta &= ((\partial_1\phi)^2-2\,\partial_1\phi+\gamma^2\cos^2\phi)\cos\theta\,\sin\theta\end{aligned} \tag{10}$$

with $\gamma^2=1+h^2$. Here, subscript 1 indicates a derivative with respect to x. All derivatives with respect to y vanish because we are working in a space of one-dimensional solutions.

To illustrate the solutions, we first consider the special case of a *flat spiral* (cycloid) with $\theta=\pi/2$. Then, the second of Eqs. (10) is automatically satisfied and the first becomes

$$\partial_1^2\phi+\gamma^2\cos\phi\sin\phi=0, \tag{11}$$

while the staggered magnetization becomes

$$\mathbf{n}=(\sin\phi,0,\cos\phi), \tag{12}$$

a cycloid that propagates along the x axis while rotating in the xz plane (upper left panel of Figs. 1 and 2). The solution for ϕ obeys

$$\partial_1\phi=\sqrt{\delta^2+\gamma^2\cos^2\phi}, \quad x=\int_0^\phi\frac{d\varphi}{\sqrt{\delta^2+\gamma^2\cos^2\varphi}}. \tag{13}$$

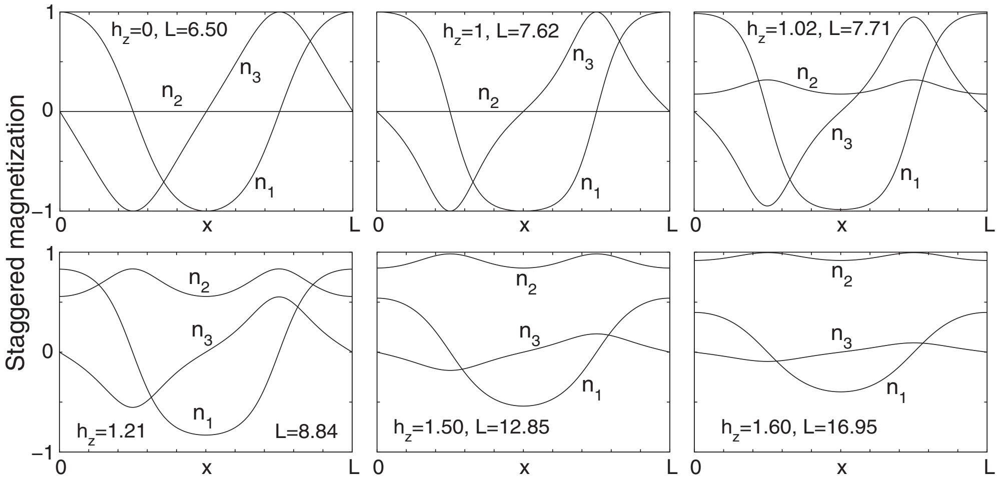

FIG. 1. Solutions of Eqs. (10) minimizing the average energy density of Eq. (18) for a number of illustrative magnetic fields $h = h_z$ pointing along the c axis. Note that the period L varies with the field. Above $h_{c2} = \sqrt{3}$ the solution becomes a commensurate antiferromagnet with $n_2 = 1, n_1 = n_3 = 0$.

The result can be expressed in terms of elliptic functions, but there is no particular advantage to doing so. δ^2 is a positive constant that will be determined below. The cycloid has a period (pitch) of

$$L = \int_0^{2\pi} \frac{d\phi}{\sqrt{\delta^2 + \gamma^2 \cos^2 \phi}} \tag{14}$$

and the free parameter δ is determined by the requirement that the average energy density $w = W/L$ achieve a minimum:

$$\frac{1}{2\pi} \int_0^{2\pi} d\phi \sqrt{\delta^2 + \gamma^2 \cos^2 \phi} = 1 \Rightarrow w = \frac{1}{2}(1 - \delta^2). \tag{15}$$

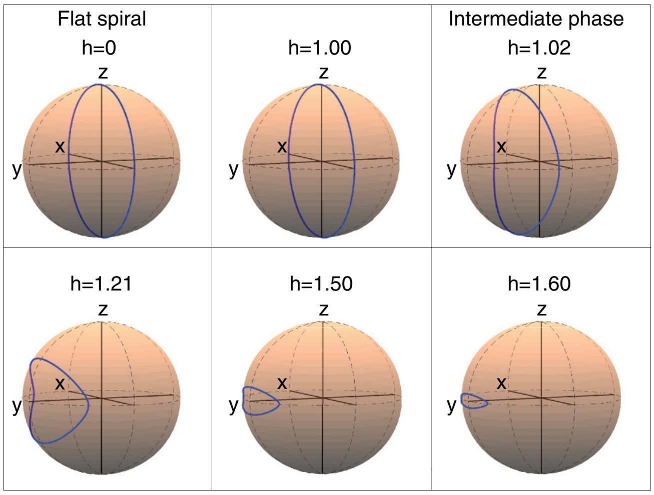

FIG. 2. (Color online) The same solutions as in Fig. 1, but viewed from a different perspective. Blue lines on the sphere surface trace out directions for the staggered magnetization, placing the base of each **n** at the center of the sphere and then moving from one unit cell to the next along x, the direction of spiral propagation. For $0 < h < h_{c1}$, the spins describe a cycle in the xz plane, while for $1 < h < h_{c2} = \sqrt{3}$, they also have a nonzero oscillating y component.

As γ (or h) increases, δ becomes zero at a critical field:

$$\gamma = \gamma_c = \pi/2 \Rightarrow h = h_c = \sqrt{\frac{\pi^2}{4} - 1} \approx 1.21. \tag{16}$$

In physical units, $H_c = 2.04$ T. This is the Dzyaloshinskii critical field and the corresponding Dzyaloshinskii scenario may be described as follows: for $h < h_c$, the solution is a flat spiral that propagates along the x axis and rotates in the xz plane. As h approaches h_c, the spiral is highly distorted and becomes a kinklike structure with diverging period. For $h > h_c$, the ground state becomes the uniform spin-flop state

$$\mathbf{n} = (1,0,0) \quad \text{modulo } U(1).$$

We realized that this scenario was incomplete when we computed the magnon spectrum[24] of the flat spiral and found negative eigenvalues starting at

$$h_{c1} = 1.01, \quad H_{c1} = 1.7 \text{ T}. \tag{17}$$

The fact that the value of h_{c1} in rationalized units is practically equal to 1 is remarkable, yet fortuitous, and bears no special significance otherwise. Above h_{c1} the flat spiral is unstable. We thus return to energy minimization and revoke the assumption $\theta = \pi/2$, although continuing to assume a one-dimensional structure of the form $\phi = \phi(x)$ and $\theta = \theta(x)$.

Efforts to find explicit analytical solutions of Eqs. (10) have not been fruitful so we resort to numerics. We minimize the energy density

$$w = \frac{1}{L} \int_0^L dx\, V(\theta,\phi) \tag{18}$$

over a periodic chain of length L and vary L to achieve a minimum for any given value of h.

For $h < h_{c1} = 1.01$, we recover the previous results for the flat spiral. But, for $h > h_{c1}$ a nonflat spiral arises with nontrivial $\phi(x)$ as well as $\theta(x)$. We call this the *intermediate state*. Examples appear in Figs. 1 and 2 for a variety of field values. Entering the intermediate phase for $h > h_{c1}$, n_2 acquires nonzero values and one can describe the state as an antiferromagnetic conical spiral that propagates along x

but nutates around y. This is precisely the structure deduced from recent scattering experiments[28,29] and called a *double-k structure* because of twofold peak characteristically observed during experimental scans through k space. As h increases, the component n_2 becomes larger and larger until at $h_{c2} = \sqrt{3}$ (or $H_{c2} = 2.9$ T), the solution becomes a commensurate antiferromagnet or spin-flop state with $\mathbf{n} = (0,1,0)$. This upper critical point was determined in Ref. 24 from a stability analysis. The existence of the intermediate state does not depend upon the presence of a nonzero transverse magnetic field.

We now comment on the two issues concerning the nature of the ground state for $h \parallel c$. Our first comment concerns the possible existence of more general structures with average energy density lower than those calculated above through the 1D ansatz (9). In particular, ground states in the form of a vortex (skyrmion) lattice in 2D Dzyaloshinskii-Moriya helimagnets have been speculated theoretically[6,7] [also in connection with $Ba_2Cu_2O_7$ (Ref. 8)], and later discovered experimentally in several such systems.[4,9–11] Hence, we carried out extensive two-dimensional simulations, but our numerical investigation yielded negative results for a potential ground state in the form of, say, a vortex lattice. Instead, in all our 2D numerical experiments, we found that the optimal configuration for $h_{c1} < h < h_{c2}$ is actually the same 1D nonflat spiral, which was obtained earlier in this section by a numerical minimization applied directly to a 1D restriction of the energy functional (18).

Second, the nonflat spiral, calculated numerically through the relaxation algorithm, exists as a stationary point of the energy functional in the region $h_{c1} < h < h_{c2}$. It is thus desirable to examine also its stability, and check whether or not there exists yet another critical field within the intermediate region, beyond which the nonflat spiral may cease to be locally stable. We have therefore calculated the magnon spectrum of the intermediate phase (Appendix A) and verified that all eigenvalues are always positive. Consequently, the nonflat spiral is locally stable within the entire intermediate region. This computation does not prove it is the ground state, but in combination with extensive numerical explorations of two-dimensional states that found no solutions of lower energy, it is a strong indication. Note that the magnon spectrum in the intermediate phase has not been experimentally investigated yet. Hence, our current theoretical predictions provide the opportunity for comparison with future inelastic neutron scattering studies.

B. Field perpendicular to *c*

We next consider a field applied in a direction strictly perpendicular to the c axis, a case that had attracted experimental interest already in Ref. 18. For the moment, we assume that the field is applied along the y axis, $\mathbf{h} = (0,h_\perp,0)$, hence the potential V of Eq. (4) reduces to

$$\begin{aligned} V = {} & \tfrac{1}{2}\left[(\partial_1\mathbf{n})^2 + (\partial_2\mathbf{n})^2 + n_3^2 + h_\perp^2 n_2^2 + 1\right] + h_\perp d_z n_1 \\ & - [(\partial_1 n_1 - \partial_2 n_2)n_3 - (n_1\partial_1 - n_2\partial_2)n_3], \end{aligned} \tag{19}$$

where the applied field enters in two distinct ways, namely, through the appearance of an effective easy-plane anisotropy $\frac{1}{2}h_\perp^2 n_2^2$ and a Zeeman-type anisotropy $h_\perp d_z n_1$. The latter also contains the strength d_z of the out-of-plane oscillating component ($\pm D_z$) of the DM vectors which was neglected in the analysis of Ref. 18.

To find minima of the energy functional, we first note that the positive term $\frac{1}{2}h_\perp^2 n_2^2$ again favors a flat-spiral configuration with $n_2 = 0$ which propagates along the x axis. Using the angular parametrization (8), we write

$$\Phi = \phi(x), \quad \Theta = \frac{\pi}{2}; \quad \mathbf{n} = (\sin\phi, 0, \cos\phi), \tag{20}$$

which is inserted in Eq. (19) to yield

$$V = \tfrac{1}{2}[(\partial_1\phi - 1)^2 + \cos^2\phi] + \bar{h}\sin\phi, \tag{21}$$

where the only free parameter

$$\bar{h} = h_\perp d_z \tag{22}$$

is a combination of the applied field $h_\perp$ and the effective out-of-plane DM anisotropy d_z.

Otherwise, the calculation is similar to that of the flat spiral in Sec. III A. Stationary points of the energy functional $W = \int V\,dx$ now satisfy the ordinary differential equation

$$\partial_1^2\phi + \cos\phi\sin\phi - \bar{h}\cos\phi = 0 \tag{23}$$

whose first integral is given by

$$(\partial_1\phi)^2 - \cos^2\!\phi - 2\bar{h}\sin\!\phi = C = 2\bar{h} + \delta^2. \tag{24}$$

Our choice of the integration constant C indicates that minimum energy is achieved with a positive new constant denoted by δ^2. The actual configuration $\Phi = \phi(x)$ is then given by the implicit equation

$$x = \int_0^{\phi} \frac{d\varphi}{\sqrt{\delta^2 + \cos^2\!\varphi + 2\bar{h}(1 + \sin\!\varphi)}}, \tag{25}$$

and the corresponding spiral period L is given by

$$L = \int_0^{2\pi} \frac{d\phi}{\sqrt{\delta^2 + \cos^2\!\phi + 2\bar{h}(1 + \sin\!\phi)}}. \tag{26}$$

Finally, the free parameter δ^2 is calculated by minimizing the average energy density $w = \frac{1}{L}\int_0^L V(x)dx$ which yields

$$\frac{1}{2\pi}\int_0^{2\pi} d\phi\sqrt{\delta^2 + \cos^2\!\phi + 2\bar{h}(1 + \sin\!\phi)} = 1, \tag{27}$$

an algebraic equation that may be used to determine δ^2 for each value of $\bar{h}$. The corresponding minimum energy is then given by

$$w = \tfrac{1}{2}(1 - \delta^2 - 2\bar{h}). \tag{28}$$

In the absence of the out-of-plane DM anisotropy ($d_z = 0$), the configuration just calculated reduces to the zero-field flat spiral of Sec. III A for any value of the applied transverse field because $\bar{h} = h_\perp d_z = 0$ for all $h_\perp$. In particular, no phase transition of the Dzyaloshinskii type would be expected to occur for a field applied in a direction strictly perpendicular to the c axis, as presumed in the analysis of early experiments.[18]

However, the situation changes significantly for $d_z \neq 0$. Then, the effective field $\bar{h} = h_\perp d_z$ is different from zero except when $h_\perp = 0$. With increasing $h_\perp$, and thus increasing $\bar{h}$, the parameter δ^2 decreases and eventually vanishes when $\bar{h}$ reaches a critical value $\bar{h} = \bar{h}_c$ computed from Eq. (26)

applied for $\delta^2 = 0$. A simple numerical calculation yields $\bar{h}_c = h_\perp^c d_z = 0.3161$, or

$$h_\perp^c = \frac{0.3161}{d_z}. \tag{29}$$

In the limit $h_\perp \to h_\perp^c$, δ^2 vanishes and the average energy density of Eq. (28) reduces to $w = \frac{1}{2}(1 - 2\bar{h}_c)$ which coincides with the energy of the uniform spin-flop state $\mathbf{n} = (-1,0,0)$. Thus, we again encounter a Dzyaloshinskii-type phase transition at a critical field that now depends on d_z.

As mentioned already, no such transition was detected in the early experiments[18] which were conducted with transverse magnetic fields of limited strength $H_\perp \lesssim 2$ T or $h_\perp \lesssim 2/1.68 \approx 1.2$. However, recent experiments[29] reveal a critical field $H_\perp^c = 9$ T or $h_\perp^c = 9/1.68 = 5.36$ and, using Eq. (29),

$$d_z = 0.06. \tag{30}$$

As far as we know, this is the first estimate of the strength of the out-of-plane DM anisotropy and will be used in all numerical calculations presented in the continuation of this paper. Incidentally, using the definition of the rationalized anisotropy $d_z = \sqrt{2} D_z / \varepsilon J$ from Ref. 24, we find $D_z/J = 0.0076$, to be compared with $\varepsilon = D_\perp / J = 0.18$.

The preceding calculation was completed in Ref. 25 with a detailed calculation of the corresponding magnon spectrum which could prove useful for the analysis of future inelastic neutron scattering experiments in the presence of a strong transverse magnetic field $H_\perp$. The same calculation reveals no sign of further critical instabilities as long as $d_z < 0.5$. In particular, an intermediate phase of the type encountered in Sec. III A is not present in the case of strictly transverse magnetic fields and $d_z < 0.5$. In other words, the predicted phase transition is of pure Dzyaloshinskii type.[20]

This section is completed with a brief discussion of the case of a transverse magnetic field

$$\mathbf{h}_\perp = h_\perp(\sin\psi, \cos\psi, 0) \tag{31}$$

which points in an arbitrary direction within the basal plane obtained by a clockwise rotation of the y axis with angle ψ (see Fig. 3). In fact, the ground-state configuration for this more general case ($\psi \neq 0$) can be surmised from the special $\psi = 0$ solution calculated earlier in this section by simple algebraic transformations, thanks to the underlying $U(1)$ symmetry of Eq. (6) broken by the applied transverse field. Indeed, let $n_1 = n_1(x)$, $n_2 = 0$, $n_3 = n_3(x)$ be the $\psi = 0$ solution. Then, the solution for $\psi \neq 0$ is given by

$$n_1' = \cos\psi\, n_1(\xi), \quad n_2' = -\sin\psi\, n_1(\xi), \quad n_3' = n_3(\xi), \tag{32}$$

where $\xi = x\cos\psi + y\sin\psi$. Thus, the new spiral propagates along the x' axis obtained by a counterclockwise rotation of the x axis with angle ψ (see Fig. 3) while the staggered magnetization rotates in the plane $x''z$ which is perpendicular to the field direction (axis y''). In other words, a flat spiral (cycloid) that initially propagates along the x axis and rotates in the xz plane ($\psi = 0$) is reoriented to propagate along the x' axis ($\psi \neq 0$) so that the normal to the spin plane (axis y'') points along the applied magnetic field. The angle formed by the direction of spiral propagation (axis x') and the normal to the spin plane (axis y'') is bisected by the conventional crystal axis $b = (0,1,0)$ denoted by a dotted line in Fig. 3 for any ψ. When the field is applied along b, $\psi = \frac{\pi}{4}$ and the normal to the spin-rotation plane is parallel to the propagation vector (screw-type spiral).

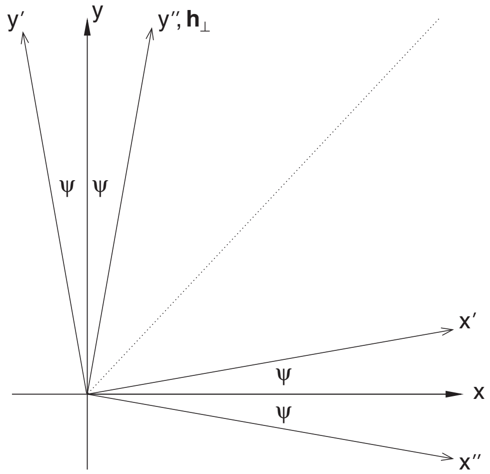

FIG. 3. Illustration of the bisection rule in a transverse field applied along the y'' axis. The spiral propagation vector points along the x' axis, while the staggered magnetization rotates in the $x''z$ plane.

The "bisection rule" just described theoretically was experimentally discovered already in Ref. 18. Actually, agreement with the ideal bisection rule requires that $H_\perp \gtrsim 0.5$ T in order to overcome a certain energy barrier due to discreteness effects which lead to an additional tetragonal anisotropy that breaks the underlying $U(1)$ symmetry even in the absence of a transverse field.[18,27] The same anisotropy explains the experimental fact that the spiral propagates along the $x = (1,1,0)$ or $x = (1,\bar{1},0)$ directions, in the absence of a transverse field, while a sufficiently strong field $H_\perp \gtrsim 0.5$ T is required to reorient the spiral according to the bisection rule.

We have thus completed the discussion of the phase diagram in the presence of a field strictly parallel to the c axis (Sec. III A) or a field strictly perpendicular to c (Sec. III B). The general case of a canted magnetic field is discussed in the following Sec. III C.

C. Canted magnetic fields

We now turn our attention to the most general case of the applied field $\mathbf{h}$, whose transverse component $h_\perp$ and the component h_z along the c axis are both nonzero. This is necessary to consider because experimentalists have reported ground-state information on the system while scanning through all field components. For a while, we assume that the magnetic field $\mathbf{h}$ is given by

$$\mathbf{h} = h_\perp \mathbf{e}_2 + h_z \mathbf{e}_3. \tag{33}$$

The explicit form of the potential of Eq. (1) becomes

$$\begin{aligned} V = {} & \tfrac{1}{2}[(\partial_1 \mathbf{n})^2 + (\partial_2 \mathbf{n})^2 + 1] \\ & - [(\partial_1 n_1 - \partial_2 n_2) n_3 - (n_1 \partial_1 - n_2 \partial_2) n_3] \\ & + \tfrac{1}{2}\gamma^2 n_3^2 + \tfrac{1}{2} h_\perp^2 n_2^2 + h_\perp h_z n_2 n_3 + h_\perp d_z n_1, \end{aligned} \tag{34}$$

where the parameter γ^2 depends upon h_z,

$$\gamma^2 = 1 + h_z^2. \tag{35}$$

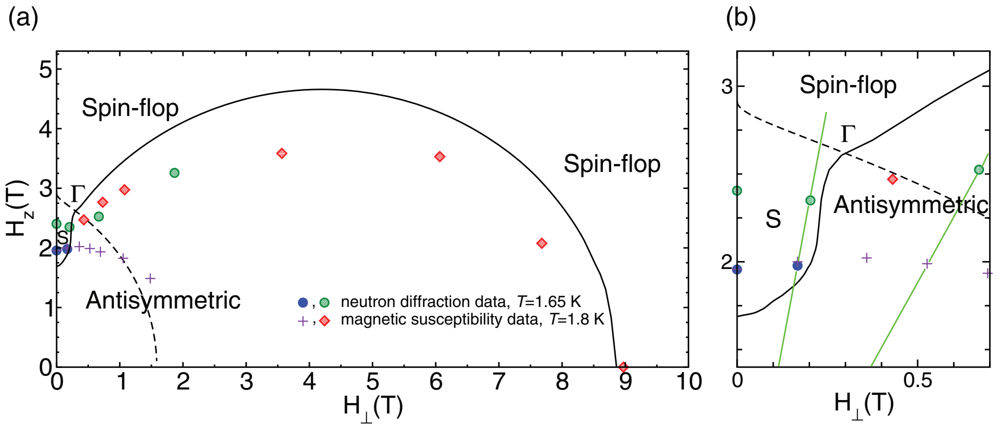

FIG. 4. (Color online) $T = 0$ theoretical prediction for the phase diagram. We adopt conventions used in publication of experiments (Ref. 29). The antisymmetric and symmetric phases reported here are illustrated in Figs. 5, 6 and 7, 9, respectively. (a) The antisymmetric phase is realized below the solid line. The symmetric phase, denoted as S in the figure, exists in the area between the solid line and the dashed line. The dashed line depicts the limit of local stability of the spin-flop phase. The spin-flop phase is locally stable above the dashed line, but is actually realized only in the area above both the dashed line and the solid line. (b) A portion of the phase diagram near the tricritical point Γ where the three phases (symmetric, antisymmetric, spin-flop) merge. Experimental data were extracted from Fig. 11(a) of Ref. 29. The straight solid (green) lines correspond to experimental scans along magnetic field that will be discussed in the paragraph on neutron scattering.

When $h_\perp \neq 0$, a brief inspection of the potential of Eq. (34) reveals that the Zeeman energy $\frac{1}{2}(\mathbf{n}\cdot\mathbf{h})^2$ now contains also the *off-diagonal* anisotropy $h_\perp h_z n_2 n_3$, which was absent when either $h_\perp = 0$ or $h_z = 0$. The presence of the latter anisotropy precludes analytical treatment. We therefore obtain the corresponding solutions by a direct minimization of the energy functional, in a manner analogous to the calculation presented in Sec. III A. For the sake of clarity, we also recall the value of the out-of-plane DM anisotropy $d_z = 0.06$ estimated in Sec. III B, which is used in all subsequent numerical calculations. We state our $T = 0$ results in the phase diagram in Fig. 4. For comparison, we include experimental critical lines determined from neutron diffraction and magnetic susceptibility measurements taken, however, at relatively high temperature $T = 1.65$ and 1.8 K.

We begin our discussion with the case where $h_z < h_{c1} = 1.01$ (or $H_z < H_{c1} = 1.7$ T) and consider the evolution of the system with increasing $h_\perp$. Our results are displayed in Figs. 5(a) and 6(a). In the limit $h_\perp = 0$, the spin configuration that minimizes the energy is the flat spiral constructed in Sec. III A. Recall that this solution is degenerate with respect to rotations around c, in agreement with the $U(1)$ symmetry given by Eq. (6). When $h_\perp \neq 0$, the $U(1)$ symmetry is broken, and the energy is minimized by a nonflat spin spiral propagating strictly along the x axis. The component of the staggered magnetization n_2 is now different from zero and points in the direction of the transverse field $h_\perp$, while its sign oscillates over the period $L = L(h_z, h_\perp)$ with the property $n_2(x) = -n_2(L - x)$. Because of this characteristic behavior, we call this state the *antisymmetric phase*. The path traced out by the staggered magnetization $\mathbf{n}$ during one period L, shown in Fig. 6(a), looks relatively simple. The spin rotates *approximately* in a plane whose normal is tilted from the y axis towards some new direction in the yz plane.

The origin of the oscillating component n_2 can be understood by a direct inspection of the Zeeman energy $\propto(\mathbf{n}\cdot\mathbf{h})^2$. Its diagonal terms $n_2^2 h_\perp^2$, $n_3^2 h_z^2$ are always positive, but the off-diagonal contribution may become *negative* provided that n_2 adjusts so that its sign is always opposite to the sign of n_3. But, the projection of $\mathbf{n}$ onto the xz plane rotates during the period L thanks to the chiral DM term $(n_1\partial_1 n_3 - n_3\partial_1 n_1)$ in

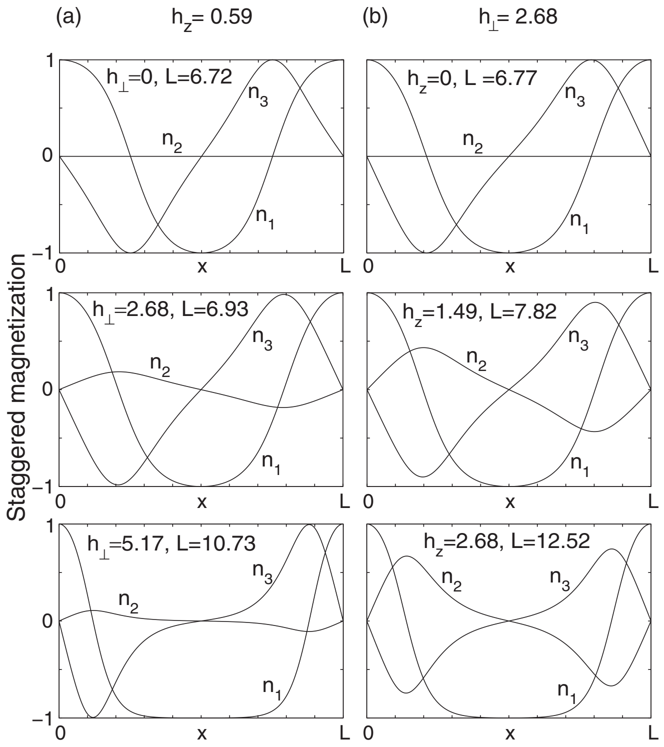

FIG. 5. Calculated evolution of spin configuration in the antisymmetric phase with the applied magnetic field. (a) Left panel: $h_z = 0.59$ ($H_z = 1$ T), $h_\perp$ increases. (b) Right panel: $h_\perp = 2.68$ ($H_\perp = 4.5$ T), h_z increases. The bottom entries in both panels are applied for points near the critical line between the antisymmetric and the spin-flop phases. Notice an enhanced $n_1 = -1$ domain in these entries. The antisymmetric spiral propagates strictly along x.

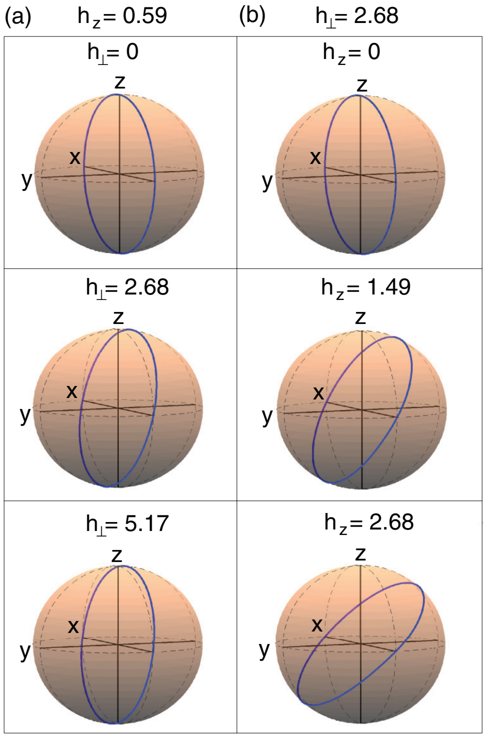

FIG. 6. (Color online) The same antisymmetric spirals as in Fig. 5 but from a different perspective. Blue lines on the sphere surface are paths traced by the end point of $\mathbf{n}$ during one period L.

the potential V of Eq. (34). Therefore, the sign of n_3 oscillates, and n_2 also displays oscillatory behavior.

To fully describe the spin structure, all terms in the potential of Eq. (34) must be considered, but the main conclusion persists: the spiral minimizes its energy by developing $n_2 \neq 0$ *along the direction of the transverse field* $h_\perp$, and the sign of n_2 oscillates over the period L. As a result, the expectation value $\langle n_2 n_3 \rangle$ becomes negative ($\langle n_2 n_3 \rangle < 0$), while $\langle n_2 \rangle = \langle n_3 \rangle = 0$, as verified by a direct calculation.

We now briefly describe the role of the term $h_\perp d_z n_1$ in Eq. (34). The importance of the latter contribution has already been established in Sec. III B during our analysis of the properties of the flat spiral ($n_2 = 0$) in the presence of a field applied strictly in the xy plane ($h_\perp \neq 0$, but $h_z = 0$). The scenario discussed in Sec. III B is here mildly modified by the presence of $h_z \neq 0$ but its main features remain the same, as confirmed by our numerical studies. The weak-ferromagnetic anisotropy $h_\perp d_z n_1$, generated by the transverse field $h_\perp$ *applied along the* y *axis*, makes the spin orientations along the $\pm x$ axis energetically nonequivalent. In the antisymmetric state, the component of the staggered magnetization that is perpendicular to the transverse field $h_\perp$ rotates in the xz plane, and is thus directly affected by the weak-ferromagnetic term $h_\perp d_z n_1$. In turn, the profile of the antisymmetric spiral is modified, and the expectation value of n_1 over the period L becomes nonzero and negative ($\langle n_1 \rangle < 0$) in order to minimize $h_\perp d_z n_1$.

With increasing $h_\perp$, the spiral becomes significantly distorted, and the $n_1 \simeq -1$ orientation (domain) during the spin rotation is greatly enhanced. This is apparent from the bottom entry of Fig. 5(a). At the same time, the period L of the spiral increases, and the energy density of the antisymmetric state begins to approach the energy density of the uniform spin-flop state $\mathbf{n} = (-1,0,0)$ from below. At the critical value of the transverse field $h_\perp^c(h_z)$, the period of the spiral grows to infinity ($L \to \infty$), and its energy density becomes equal to the energy density of the spin-flop state $w = \frac{1}{2}(1 - 2h_\perp d_z)$. This numerically verified scenario is consistent with experiment,[29] and is somewhat similar to that discussed in Sec. III B for strictly transverse fields. Above the critical line, only the uniform spin-flop state emerges from our numerical calculations, and the incommensurate antisymmetric spiral no longer exists. The boundary between the antisymmetric and the spin-flop states is indicated by the solid line in Fig. 4. We have verified that the antisymmetric state displayed in the phase diagram always carries lower energy density than the uniform spin-flop state.

Evolution of the spin structure with increasing h_z, but fixed strength of the transverse field $h_\perp$, is shown in Figs. 5(b) and 6(b). Our results, applied here for $h_\perp = 2.68$ ($H_\perp = 4.5$ T), are qualitatively similar to those in Figs. 5(a) and 6(a). In particular, the spiral again develops a nonzero oscillating component $n_2 \neq 0$ along $h_\perp$, with zero expectation value $\langle n_2 \rangle = 0$ over the period L. Expectation value $\langle n_2 n_3 \rangle < 0$ due to the off-diagonal anisotropy $n_2 n_3 h_\perp h_z$, whereas $\langle n_1 \rangle < 0$ thanks to the weak-ferromagnetic term $h_\perp d_z n_1$. With increasing h_z, the period of the spiral L increases and presumably again diverges ($L \to \infty$) at the critical line. Above the critical line, only the uniform spin-flop state emerges from our numerical calculations, and the incommensurate antisymmetric spiral no longer exists.

We emphasize that the characteristic properties of the antisymmetric state discussed in the preceding paragraphs remain the same for *any point* $h_z \neq 0$, $h_\perp \neq 0$ below the solid line in Fig. 4. However, the scenario of the phase transition between the antisymmetric and the spin-flop phases, discussed in connection with Fig. 5, is slightly modified for sufficiently weak $h_\perp$, near the point Γ. Specifically, for $H_\perp$ below ~1 T, the energies of both states again become equal at the critical line, but the period L of the antisymmetric spiral remains *finite* (albeit large). Above the critical line, our numerical minimization still yields the solution in the form of the antisymmetric spiral with, however, the energy density higher than the energy density of the spin-flop state $\mathbf{n} = (-1,0,0)$. This should be contrasted with behavior for large $h_\perp$, where the period of the antisymmetric spiral *diverges* ($L \to \infty$) at the critical line; and above the critical line, only the uniform spin-flop state exists. Interestingly, our results seem to be again consistent with the experiment.[29]

We now focus on the area left from the point Γ in the phase diagram. Our spin-wave analysis of the spin-flop state in the presence of arbitrary canted fields, given in Appendix B, established that the spin-flop phase is locally unstable below the dashed line in Fig. 4. Thus, it can not exist beyond the point Γ, where the energy densities of the antisymmetric and the spin-flop states become equal. It is more or less clear that there is a new phase realized in some area just below the dashed line, near the axis h_z (near $h_\perp = 0$). Note that the dashed line starts from the point $h_z = \sqrt{3}$ ($H_z = 2.9$ T), which is just the upper critical field h_{c2} obtained in Ref. 24. For $h_z < h_{c2}$, the spin-flop phase is locally unstable, and the intermediate

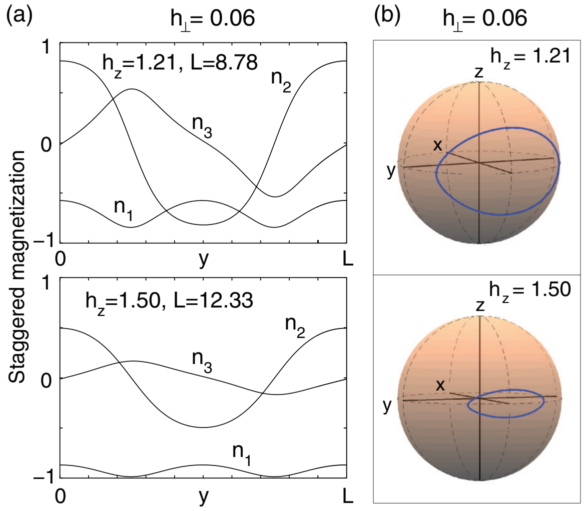

FIG. 7. (Color online) (a) Examples of spin configurations in the symmetric phase, calculated for $h_\perp = 0.06$ (or 0.1 T) and the two values of h_z. This phase exists in the narrow area of the phase diagram $1.01 \lesssim h_z \lesssim \sqrt{3}$ ($1.7\,\mathrm{T} < H_z < 2.9\,\mathrm{T}$) and weak but nonzero $h_\perp$, $0 < h_\perp \lesssim 0.12$ ($0 < H_\perp \lesssim 0.2$ T). The symmetric conical spiral propagates strictly along y and nutates around the $-x$ axis. Otherwise, its properties are similar to its precursor phase, the intermediate state of Sec. III A. (b) The same symmetric spirals viewed from a different perspective. Blue lines on the sphere surface are paths traced by the end point of $\mathbf{n}$ during one period L.

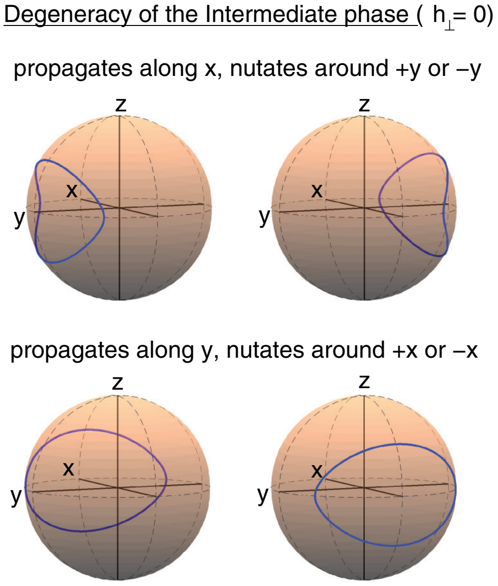

FIG. 8. (Color online) Illustration of the four degenerate states in the intermediate phase ($h_\perp = 0$) discussed in the text, calculated here for $h_z = 1.21$. Thick lines on the sphere indicate paths traced out by the end points of the staggered magnetization during one period L. The base of the staggered magnetization is placed at the center of the sphere. A nonzero transverse component $h_\perp \neq 0$, applied along $+y$, breaks the above degeneracy and favors the spiral propagating along y and nutating around the $-x$ axis, which becomes the precursor of the symmetric spiral.

phase is realized in the region $h_{c1} < h_z < h_{c2}$. It is natural to expect that the intermediate phase survives in some form also in the presence of a weak transverse field $h_\perp \neq 0$.

Our calculations confirm this expectation. When $h_\perp \neq 0$, a *symmetric phase* emerges as the ground state in the region between the dashed and the solid lines in Fig. 4. This phase acquires its name because $n_1(y) = n_1(L/2 + y)$. Two examples are illustrated in Fig. 7. The symmetric phase can be described as an antiferromagnetic conical spiral that propagates *strictly along* y, but nutates around the $-x$ axis. Importantly, the component n_1, *perpendicular* to the transverse field $h_\perp$, is nonzero ($n_1 \neq 0$) and always negative ($\langle n_1 \rangle < 0$). All these features agree with the experiment.[29]

The symmetric phase develops from its predecessor, the intermediate phase (the conical antiferromagnetic spiral) discussed in Sec. III A for fields strictly parallel to c. Recall that the intermediate phase obeys the $U(1)$ symmetry described by Eq. (6). In practice, the $U(1)$ symmetry is broken by an additional tetragonal anisotropy induced by discreteness effects.[18,27] Thus, in the absence of transverse fields, there exist four degenerate states, shown in Fig. 8: the conical spiral propagates along x and nutates around the $\pm y$ axis or it propagates along y but nutates around the $\pm x$ axis.

This degeneracy is broken when $h_\perp \neq 0$. To illustrate this point, consider for a moment the intermediate spiral with the profile $\mathbf{n}$, calculated in the absence of a transverse field. Inserting this solution in the potential V of Eq. (34), applied with $h_\perp \neq 0$, yields the additional corrections to the energy given by $\frac{1}{2}h_\perp^2\langle n_2^2\rangle + h_\perp d_z\langle n_1\rangle$. The first correction, quadratic in $h_\perp$, originates in the Zeeman energy $\propto(\mathbf{n}\cdot\mathbf{h})^2$. Note that the off-diagonal Zeeman term $h_\perp h_z\langle n_2 n_3\rangle$ does not contribute because the expectation value $\langle n_2 n_3\rangle$ in the intermediate phase vanishes for any degenerate state. The second correction, linear in $h_\perp$, is due to the weak-ferromagnetic anisotropy $d_z(\mathbf{h}\times\mathbf{e}_3)\cdot\mathbf{n}$. This linear contribution dominates for small transverse field, and favors the particular degenerate state, namely, the conical spiral propagating along y and nutating around the $-x$ axis, with $\langle n_1\rangle < 1$. Numerical work confirms that the above qualitative argument is correct despite the simplifying assumption that neglects the changes in the staggered magnetization induced by $h_\perp$. The actual profile of the symmetric spiral $\mathbf{n}$ and its period L are both mildly modified by $h_\perp \neq 0$. Otherwise, its properties are similar to the intermediate phase.

The symmetric phase emerges in canted magnetic fields applied nearly parallel to the c axis, when $h_z \gtrsim h_{c1}$. It is the stationary point of the energy functional with the lowest-energy density in the area between the dashed line and the solid line of Fig. 4. With increasing h_z, the period L increases, and the magnitude of n_1 becomes larger and larger, until at the dashed line $n_1 \to -1$ and the solution becomes the spin-flop state $\mathbf{n} = (-1,0,0)$. This behavior, apparent also from Fig. 7, is virtually identical to the intermediate phase. Our results generally agree with experimental findings.[28,29] Evolution of the spin structure with increasing $h_\perp$ but fixed strength of the longitudinal component h_z is rather mild. The period L slightly decreases with $h_\perp$, whereas the magnitude of n_1 moderately increases due to the weak-ferromagnetic energy $d_z(\mathbf{h}\times\mathbf{e}_3)\cdot\mathbf{n}$. Importantly, at the critical solid line, the energy density of the symmetric phase becomes equal to the energy density of the antisymmetric phase. This happens at $h_\perp \sim 0.12$ or 0.2 T.

For stronger $h_\perp$, the antisymmetric state emerges as the true ground state, with the energy density lower than the symmetric spiral. The corresponding phase transition is first order, and is further discussed in the following paragraphs.

Comparison with neutron diffraction. Experimental data were obtained from measurements with a magnetic field of varying strength H applied at an angle α with respect to the c axis[28,29] [see the straight (green) lines in Fig. 4]. The in-plane component of the field $H_\perp = H \sin\alpha$ was directed along the y axis, or the $(-1,1,0)$ axis using the notation of Refs. 28 and 29. The alternative choice $H_\perp \parallel (1,0,0)$ yielded equivalent results, and is thus ignored in the following discussion. We concentrate on the data for $\alpha \sim 5^\circ$ and 15°, analyzed in detail in Ref. 29. We used similar angles 4.57° and 15.64° in our calculations.

We first discuss the case $\alpha \sim 5^\circ$. For $H < H_{c1}(\alpha) = 1.95$ T, the experiment observed an incommensurate structure that propagates along y, while its spin rotates in the xz plane, perpendicular to $H_\perp$. This structure is a cycloid for weak H, that distorts to a soliton lattice for stronger fields. At the critical field H_{c1}, the propagation direction suddenly rotates exactly by $\pi/2$, from the y to the x axis, and the structure becomes an antiferromagnetic cone.[28,29] This antiferromagnetic cone phase (or the double-k phase) propagates along y, parallel to $H_\perp$. Its "incommensurate" spin component rotates in the yz plane, while a "commensurate" component is perpendicular to both the c axis and the transverse field, as shown in Fig. 13(a) in Ref. 29. Finally, the IC transition is observed at $H_{c1} \approx 2.4$ T.

These experimental findings are consistent with our results. For $H < H_{c1}$ [the top entry in Fig. 9(a)], theory predicts the antisymmetric phase that propagates strictly along x, perpendicular to $H_\perp$. Importantly, the component of the staggered magnetization n_2, oscillating along $H_\perp$, is for $\alpha \sim 5^\circ$ rather small, and the structure resembles the flat spiral. The antisymmetric phase can be identified with the cycloid and/or the soliton lattice of Ref. 29. Above $H_{c1}(\alpha)$, predicted at $\sim$1.9 T, the symmetric phase, a conical spiral propagating along y but nutating along the $-x$ axis, emerges [see the middle and the bottom entries in Fig. 9(a)]. This agrees with the spin structure proposed in Ref. 29, and the symmetric phase should be identified with the antiferromagnetic cone phase. The IC transition occurs at $H_{c2}(\alpha) \sim 2.7$ T. Note that the antisymmetric spiral propagates strictly along the x axis, while the symmetric propagates along y. Therefore, the phase transition at H_{c1} is accompanied by a sudden rotation of the spiral propagation direction exactly by $\pi/2$, as in the experiment. This sudden $\pi/2$ rotation, highlighted as a noteworthy feature of recent experiments, has been explained by our previous analysis earlier in this section. Specifically, the presence of $H_\perp \neq 0$ breaks the $U(1)$ symmetry described by Eq. (6), and selects a particular spin orientation and spiral propagation direction in each phase. Thus, in the antisymmetric phase, propagation along x is required to minimize the Zeeman energy, while the symmetric phase must propagate along y in order to minimize the dominant weak-ferromagnetic contribution $d_z(\mathbf{h} \times \mathbf{e}_3) \cdot \mathbf{n}$. In this respect, we note that the sudden $\pi/2$ rotation should only occur when $H_\perp \neq 0$, and is not expected for $\alpha = 0$ or fields applied strictly along the c axis. However, a perfect alignment of the applied field with the c axis is impossible to achieve in practice. Therefore, the results of Ref. 28 reported for $\alpha = 0$ and "a sample with an almost perfect alignment" (misalignment less than 0.5°) should be interpreted from the perspective of our previous comment.

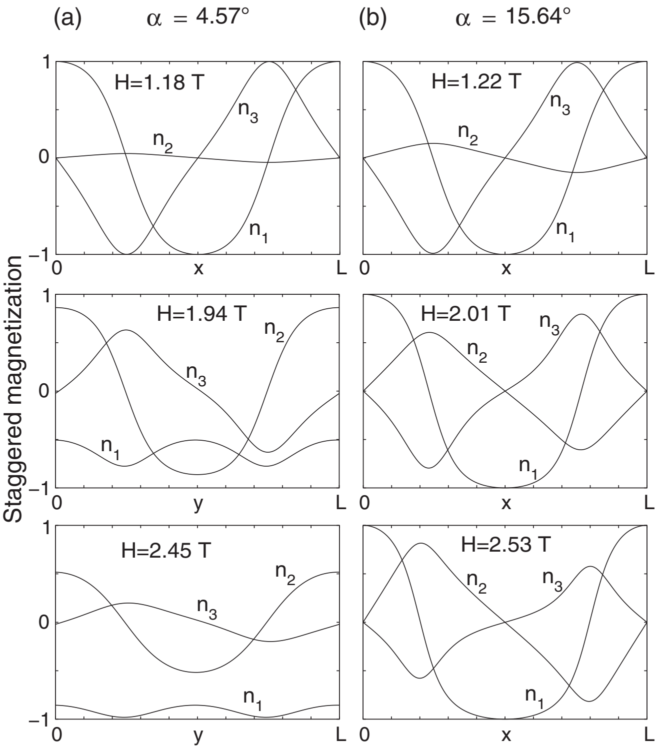

FIG. 9. Calculated spin configurations in a magnetic field of varying strength H, applied at an angle α with respect to the c axis. The two values of α are roughly equal to 5° and 15° used in neutron scattering measurements of Ref. 29. (a) $\alpha = 4.57^\circ$. The top entry corresponds to the antisymmetric phase, and the spiral propagates along x. The middle and the bottom entries display the symmetric phase, where the spiral propagates along y. Phase transition between the antisymmetric and the symmetric phases is accompanied by sudden $\pi/2$ rotation of propagation direction. (b) $\alpha = 15.64^\circ$. All entries show the antisymmetric phase, with propagation direction along x.

We now discuss the evolution of the incommensurability parameter $L(0)/L(H)$, shown in Fig. 10(a). Note a discontinuous jump of the incommensurability parameter to higher value at the critical field H_{c1}, considered as another characteristic feature of the phase transition to the antiferromagnetic cone phase.[29] We emphasize a remarkable agreement of our theory with the experimental data; the incommensurability parameter increases by $\sim$5% (theory) or $\sim$6% (experiment). The calculated value of $H_{c1} \sim 1.89$ T also agrees well with $\sim$1.97 T extracted from the experimental data. Note that the latter value, obtained from our analysis of the experiment, differs from 1.95 T quoted in Ref. 29. The calculated critical field $H_{c2} \sim 2.7$ T is slightly larger than the observed $\sim$2.4 T. However, the overall agreement is good. One should keep in mind that we compare the $T = 0$ calculations with the data taken at relatively high temperature $T = 1.65$ K $\sim 0.5T_N$. Actually. our theoretical data are shown only for field values up to 2.6 T $< H_{c2}$. This is because of numerical difficulties that occur as the period L rapidly quickly grows near H_{c2}. The corresponding average energy density, which is a

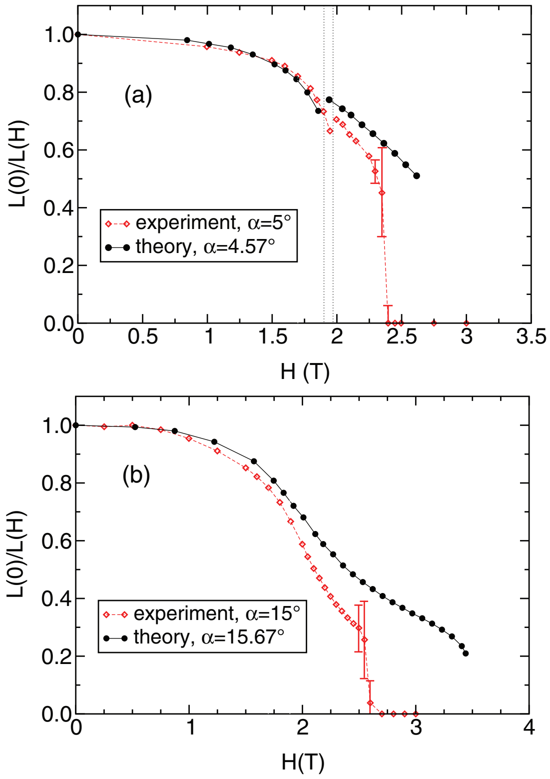

FIG. 10. (Color online) Evolution of the incommensurability parameter $L(0)/L(H)$ with the strength of the magnetic field applied at an angle α with respect to the c axis. Comparison of $T = 0$ theoretical predictions with experiment. Neutron scattering data and error bars, taken at $T = 1.65$ K, were extracted from Fig. 10 of Ref. 29 and adjusted to fit our conventions. (a) $\alpha \approx 5^\circ$. The two dotted lines mark the location of the critical field $H_{c1}(\alpha)$ determined by theory (1.9 T) and experiment (1.97 T). A discontinuous jump to a larger value at H_{c1} corresponds to the phase transition between the antisymmetric and the symmetric phases. (b) $\alpha \approx 15^\circ$.

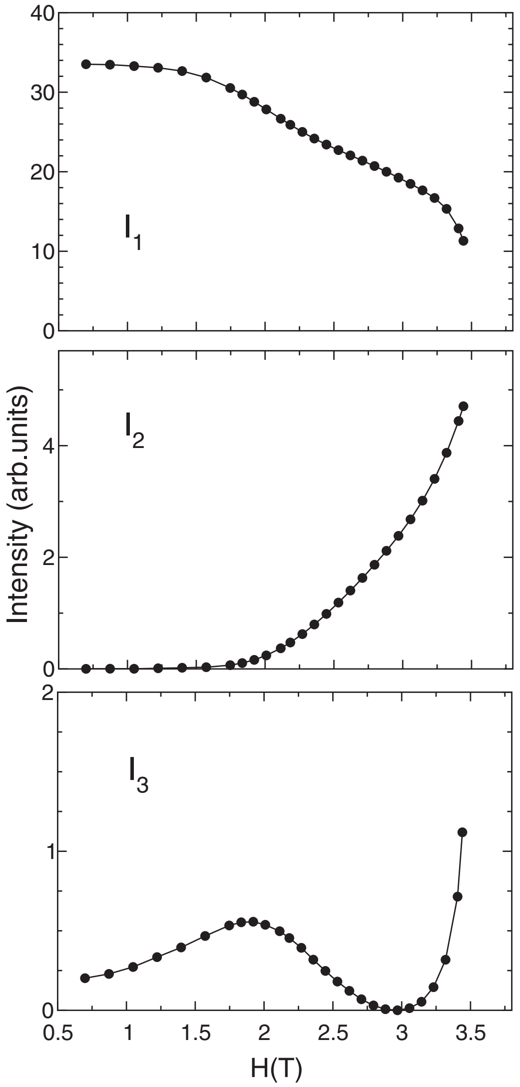

FIG. 11. Theoretical field dependence for the intensities of the first, second, and the third Fourier harmonics calculated from the n_1 and n_3 components of the staggered magnetization. The magnetic field was H was applied at an angle $\alpha = 15.64^\circ$ with respect to the c axis and is roughly equal to 15° used in the expermental Fig. (8), Ref. 29. We adopt SI units to facilitate comparison with the experiment.

function of L, then displays a shallow minimum that makes it hard to determine the precise value of L. Nevertheless, our calculations indicate a continuous IC transition with $n_1 \to -1$, but *finite* (albeit large) L in the limit $H \to H_{c2}$.

We now discuss the case when the field is applied at "large" angle $\alpha \sim 15^\circ$ with respect to the c axis. In this case, no reorientation of the spiral propagation direction (which is along x) was observed in the experiment.[29] For $H \gtrsim 1.7$ T, the proposed spin structure was described as clearly nonsinusoidal, nonplanar "complexly distorted incommensurate phase," whose detailed structure, however, remained unresolved. This "distorted incommensurate phase" was characterized by the smooth appearance of higher-order harmonics seen by neutron diffraction, both odd and even. The measured dependence of the incommensurate parameter on H displays a characteristic shape, concave for weak field, and convex when $H \gtrsim 1.7$ T. Finally, the IC transition is observed at ∼2.6 T. All these features are consistent with our $T = 0$ calculations, which predict the antisymmetric phase with oscillating $n_2 \parallel H_\perp$, propagating along x for all field strengths until the IC transition at ≈3.45 T. Predicted critical field is somewhat larger than that observed in the experiment, but is not terribly inconsistent with the measured value 2.6 T quoted in Ref. 29, especially in view of our previous comments. The n_2 component is small for weak fields, but its magnitude quickly increases with H, as apparent from Fig. 9(b). For stronger fields, the calculated structure becomes clearly nonsinusoidal, nonplanar, and can be identified with the "distorted incommensurate structure" of Ref. 29. Importantly, the Fourier transform of the staggered magnetization provides evidence for higher harmonics, both odd and even.

Our $T = 0$ theoretical results for the field dependence of the *intensities* of the first, second, and third Fourier components of the staggered magnetization $\mathbf{n}(x)$ are presented in Fig. 11. The intensities are calculated from the n_1, n_3 components. This is because neutron scattering sees only the components perpendicular to momentum transfer (which is parallel to n_2). Our results are related to the experimental data in Fig. 8(b) of

Ref. 29. The first harmonic displays the typical shape seen in the experiment: first very mild, almost linear decrease followed by a convex shape for $H \gtrsim 1.7$ T that becomes concave near the IC critical field. The difference with experiment thus lies mainly in somewhat larger theoretical value of the IC critical field, as mentioned already in the previous paragraph. In agreement with the observation, higher harmonics smoothly appear above 1.7 – 2 T. The intensity of second harmonics linearly increases with the field, as in the experiment. Similarly, the third harmonics first increases, then shows a shallow dip and increases again near the IC critical field. This characteristic behavior is exactly what was observed in the experiment.[29] On the other hand, our results show rapid increase of both higher harmonics as the field approaches the critical value, whereas the experimental data show smoothing at the IC transition. This can be perhaps due to finite temperature. Overall agreement with experiment is, however, fairly good.

Finally, we discuss the field dependence of the incommensurability parameter shown in Fig. 10(b). In agreement with experiment, the curve shows no discontinuity until the IC transition. The shape is concave for weak field strengths, but becomes convex for $H \gtrsim 1.7$ T. This corresponds to the emergence of higher harmonics and is again in agreement with the experiment, with minor discrepancy in the value of the IC critical field. The nature of the observed IC transition as deduced from the measured incommensurability parameter remains unclear; the corresponding wording in Ref. 29 (page 9) suggests that the data are consistent with a discontinuous transition. However, the related discussion in page 8 of the same reference states that due to the smallness of the measured parameter near the critical field, “no reliable conclusion can be drawn” whether the data continuously diverge or show a finite jump. In any case, for $\alpha = 15^\circ$ our calculations indicate a discontinuous IC transition, which becomes continuous for larger angles. This point has already been briefly discussed in the discussion of the antisymmetric spiral.

Comparison with magnetic susceptibility measurements. Neutron scattering studies confirmed the existence of the double-k phase and proved useful for examination of its properties. However, they were limited to only few values $\alpha = 0^\circ$, 5°, 15°, and 30°. Thus, the exact boundaries of the double-k phase (or the symmetric phase) remain an open question. For example, our theory predicts that the latter phase exists for $\alpha \lesssim 6^\circ$, which is just slightly above the experimentally studied case 5°. Additional measurements in the region $5^\circ < \alpha < 10^\circ$ may help to clarify this issue.

The phase diagram was further explored by complementary magnetic susceptibility measurements. Peaks in the experimental data, taken at $T = 1.8$ K, yielded the two critical “lines” marked in the phase diagram of Fig. 4 by crosses and diamonds. Near the c axis ($\alpha = 0^\circ$ and 5°), a single sharp peak in the data was interpreted as the transition to the double-k phase at H_{c1}. The results were practically identical with neutron scattering studies, as apparent from the overlap of the first two crosses with neutron diffraction data. The IC transition at H_{c2} is featureless in magnetic susceptibility.

However, for $\alpha \geqslant 10^\circ$, a single peak splits into two. The lower peak (crosses) is interpreted as a crossover to a “distorted incommensurate structure” seen in magnetic diffraction. The nature of this “distorted structure” has already been discussed in previous paragraphs. The lower peak broadens with increasing α, and completely disappears at $\alpha \sim 45^\circ$. The sharp upper peak (diamonds) is clearly seen until $\alpha \sim 90^\circ$ corresponds to the IC phase transition between the antisymmetric and the spin-flop phases. The agreement between our $T = 0$ theory and the experiment is almost perfect for $\alpha \sim 90^\circ$ or the fields applied strictly in the xy plane. This is not surprising because the measured critical field 9 T was actually used as an input value in our theoretical estimate of the out-of-plane DM anisotropy d_z. The slight discrepancy in the critical field for strictly transverse field, seen in the phase diagram of Fig. 4, is simply due to the fact that we adopted the rounded value $d_z = 0.06$ that differs by $\sim 10^{-3}$ from the exact result. For canted fields, our theory predicts somewhat larger critical fields than those measured in the experiment. However, the overall agreement is satisfactory, and discrepancies in the values of the critical fields are typically ∼10–20%.

We end this section with two comments:

(i) Numerical work confirms that the existence of $d_z \neq 0$ is not crucial for the appearance of the *double-k structure* and/or sudden $\pi/2$ rotations observed in experiment. It is, however, important to provide quantitative agreement with experiment. In particular, for $d_z = 0$ and fields nearly parallel to c, the intermediate phase would first appear at h_{c1} in the form of a nonflat spiral propagating strictly along x but nutating around the y axis, *without* reorientation of the spin propagation direction. A sudden $\pi/2$ rotation of the propagation direction occurs later, at yet another critical field $h_{\text{rotation}} \approx 1.20$, above which the minimum energy state becomes the symmetric spiral propagating along y but nutating around the x axis. In the absence of the weak-ferromagnetic energy $d_z(\mathbf{h} \times \mathbf{e}_3) \cdot \mathbf{n}$, an explanation of sudden reorientation requires a detailed analysis of the of the energy term $\propto (\mathbf{n} \cdot \mathbf{h})^2$.

(ii) We assumed that the transverse component of the field $h_\perp$ points strictly along the y axis. Our results, however, are not restricted to this special case. For example, assume that $h_\perp$ points in an arbitrary direction in the xy plane, which is obtained by a clockwise rotation of the y axis with angle ψ. Then, the staggered magnetization $\mathbf{n}$ for any state calculated earlier in this section must be also rotated clockwise with the angle ψ around the c axis, while the original direction of spin propagation must be rotated counterclockwise, with the angle $-\psi$. All other results remain unchanged.

IV. CONCLUSION

We have presented a rather complete theoretical study of $T = 0$ phase transitions in canted fields of arbitrary strength and direction. We calculated the complete phase diagram and identified the symmetries of states in a number of different regions. For the fields applied nearly parallel to the c axis, we confirmed the existence and stability of the intermediate phase that mediates the incommensurate-commensurate transition and analyzed its properties. We identify this phase with an experimentally observed *double-k structure*. By analyzing data on fields applied perpendicular to the c axis, we determine an out-of-plane anisotropy parameter d_z needed to complete quantitative comparison with experiment. Finally, our model accounts for sudden $\pi/2$ rotations that have been highlighted as a noteworthy feature of recent experiments.

The work reported in this paper results from a longstanding theoretical investigation of spiral magnetic structures in Dzyaloshinskii-Moryia antiferromagnets. The theoretical framework involves a number of approximations: the replacement of quantum-mechanical by classical variables, ignoring interlayer couplings and the replacement of discrete spins by continuous fields in a model Lagrangian.

Nevertheless, detailed agreement with experiment[28,29] is now so extensive that the applicability of this model to systems such as $Ba_2CuGe_2O_7$ may now be established. The only remaining discrepancies lie in the particular magnetic field values at which transitions between magnetic states take place. These discrepancies are on the order of 10%–20%, which is not much beyond experimental uncertainty. The discrepancies can also be partly attributed to the fact that the experimental data were taken at relatively high temperature $\sim 0.5T_N$.

ACKNOWLEDGMENTS

This work was partially supported by ESF Research Networking Programme POLATOM. J.C. gratefully acknowledges the support by the Slovak Research and Development Agency under the Contract No. APVV-0027-11. M.M. acknowledges partial support also from the US National Science Foundation through Grant No. DMR1002428. The work of N.P. has been co-financed by the European Union (European Social Fund, ESF) and Greek national funds through the operational program Education and Lifelong Learning of the National Strategic Reference Framework (NSRF) under "Funding of proposals that have received a positive evaluation in the 3rd and 4th Call of ERC Grant Schemes."

APPENDIX A: MAGNON SPECTRUM FOR *h* ∥ *c*

Here, we calculate the magnon spectrum of the intermediate state from Sec. III A. We first introduce new fields according to

$$\begin{aligned}\Theta(x,y,t) &= \theta(x) - g(x,y,t),\\ \Phi(x,y,t) &= \phi(x) + f(x,y,t)/\sin\theta(x),\end{aligned} \tag{A1}$$

where θ and ϕ are solutions for the intermediate state found previously in Sec. III A, and f and g account for small fluctuations. The new fields (A1) are introduced in the complete Lagrangian given by Eq. (4) applied with $\mathbf{h} = (h,0,0)$ which is then expanded to second order in f and g.

The final result for the linearized equations of motions is

$$\begin{aligned}\left(\partial_1^2 + \partial_2^2 - \partial_0^2\right) f &= U_{11} f + U_{12} g + A\partial_1 g + B\partial_2 g + C\partial_0 g,\\ \left(\partial_1^2 + \partial_2^2 - \partial_0^2\right) g &= U_{22} g + U_{21} f - A\partial_1 f - B\partial_2 f - C\partial_0 f,\end{aligned} \tag{A2}$$

where all functions except f and g are functions only of x and are given by

$$\begin{aligned}U_{11} &= -(\partial_1\theta)^2 + \cos^2\theta((\partial_1\phi)^2 - 2\,\partial_1\phi)\\ &\quad + \gamma^2(\cos^2\phi\cos^2\theta - 2\cos^2\phi + 1),\\ U_{12} &= -\frac{(2\,\partial_1\phi - 2)\,\partial_1\theta}{\sin\theta},\\ U_{21} &= \frac{(2\,\partial_1\phi - 2)\cos^2\theta\,\partial_1\theta + 2\gamma^2\cos\phi\sin\phi\cos\theta\sin\theta}{\sin\theta},\\ U_{22} &= -((\partial_1\phi)^2 - 2\,\partial_1\phi + \gamma^2\cos^2\phi)(2\sin^2\theta - 1),\\ A &= (2\,\partial_1\phi - 2)\cos\theta, \quad B = -2\sin\phi\sin\theta,\\ C &= -2h\cos\phi\sin\theta.\end{aligned} \tag{A3}$$

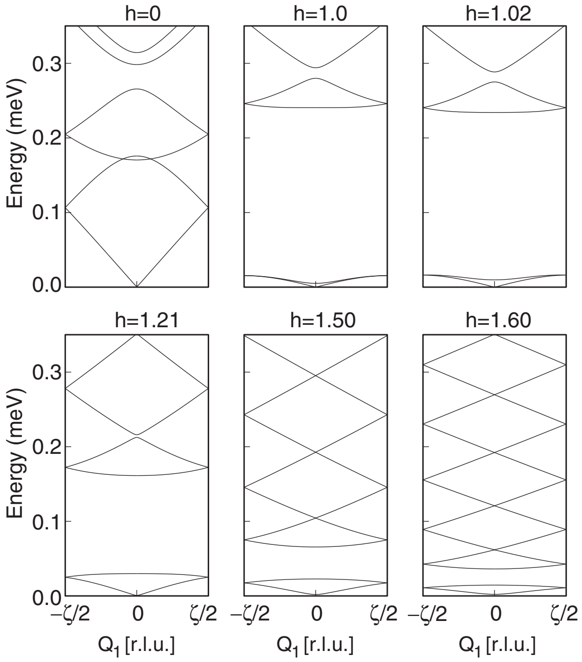

FIG. 12. Magnon spectrum along the x direction in the reduced zone scheme for six illustrative magnetic fields. For $h > h_{c1} = 1.01$, the results show the magnon spectrum of the intermediate phase. The wave number Q_1 is measured in relative lattice units defined as $\zeta = \varepsilon/L = 0.1774/L$. Note that the lowest-lying band has a linear dispersion relation.

We have verified that for the flat spiral ($\theta = \pi/2$, $\partial_1\phi = \sqrt{\delta^2 + \gamma^2\cos^2\phi}$), these expressions reduce to those previously obtained for the magnon spectrum of the flat spiral in Eq. (5.2) of Ref. 24, but with $\phi \longleftrightarrow \theta$. Note that the two linear equations for f and g are coupled as long as the magnetic field h is different from zero or spin-wave propagation deviates from the x axis.

We have solved the linear system (A2) by a Bloch analysis of the type given in Appendix A of Ref. 24 now extended to calculate the low-energy magnon spectrum throughout the intermediate phase $h_{c1} < h < h_{c2}$. The numerical procedure yields eigenfrequencies $\omega(q_1,q_2)$ as functions of Bloch momentum $\mathbf{q} = (q_1,q_2)$. Since the potential terms on the right-hand side of Eq. (A2) are periodic along x with period L, the component q_1 of the Bloch momentum can be restricted to the zone $[-\pi/L,\pi/L]$. But, q_2 is unrestricted because the background spin spiral is independent of y.

We present the results of the magnon calculations in Figs. 12 through 14. The Bloch momentum in the figures is quoted in relative lattice units $\mathbf{Q}$[r.l.u.]$= (\varepsilon/2\pi)\mathbf{q} = 0.028\mathbf{q}$, following conventions in publication of experiments. Note that the value $\mathbf{Q}$[r.l.u.]$= 1$ corresponds to Bloch wavelength of one lattice spacing of the square lattice formed by the Cu atoms within each layer. The component Q_1 along the x axis can now be restricted to the zone $[-\zeta/2,\zeta/2]$, where $\zeta = \varepsilon/L = 0.1774/L$.

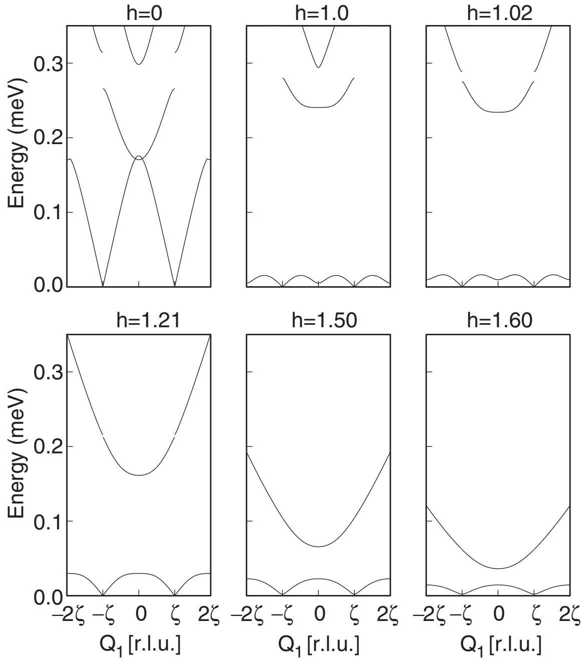

FIG. 13. Magnon spectrum along the x direction in the extended zone scheme for six illustrative magnetic fields. For $h > h_{c1} = 1.01$, the results show the magnon spectrum of the intermediate phase. Bands have been assembled in a fashion that corresponds with conventions in publication of experiments.

We make the following comments:

(i) All eigenvalues are positive. Therefore, the intermediate state is locally stable. This computation does not prove it is the ground state, but in combination with extensive numerical explorations of two-dimensional states that found no solutions of lower energy, it is a strong indication.

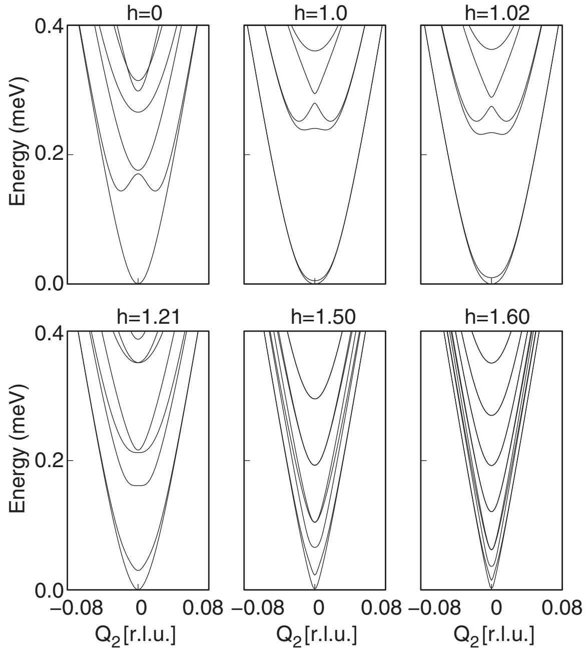

FIG. 14. Magnon spectrum along the y direction for six illustrative magnetic fields. For $h > h_{c1} = 1.01$, the results show the magnon spectrum of the intermediate phase. The wave number Q_2 is measured in relative lattice units explained in the text.

(ii) We provide plots both in the reduced zone scheme and the extended zone scheme. The reduced zone scheme is more compact, particularly for h_{c1} and below. However, as the field increases towards h_{c2}, the reduced zone scheme acquires a large number of bands that are resolved more clearly in the extended zone scheme. Experimentalists are likely to find the display in the extended zone scheme more useful.

(iii) Along Q_1, the low-energy spectrum is linear at the zone center. Moving towards h_{c2} it acquires two bands: an "acoustic" band with linear dispersion and an upper optical band (higher bands exist that have not been resolved by the computation). The linear portion of the acoustic band is the Goldstone mode of these magnetic spin states. In the limit that $h \to h_{c2}$ the bands depicted here collapse onto the horizontal axis; the next excitation is at an energy over 0.4 that lies above the top of the figure.

(iv) Along Q_2, the low-energy spectrum is quadratic. As h increases towards h_{c2} the quadratic regions become small and the spectrum becomes nearly linear. Upon reaching h_{c2}, the dispersion becomes completely linear. At this point, it produces the Goldstone mode of the spin-flop phase.

APPENDIX B: LOCAL STABILITY OF THE SPIN-FLOP PHASE IN CANTED MAGNETIC FIELDS

Here, we calculate the magnon spectrum of the spin-flop phase in the presence of canted magnetic field given by Eq. (8) and thus examine an important issue concerning its stability.

We first note that the uniform spin-flop state $\mathbf{n} = (-1,0,0)$, or $\Phi = -\frac{\pi}{2}$, $\Theta = \frac{\pi}{2}$ using the spherical parametrization (8), is a more or less obvious stationary point that minimizes the energy functional $W = \int V\,dx\,dy$, where V is the potential given in Eq. (34). Actually, there exist two different spin-flop configurations $\mathbf{n} = (\mp 1,0,0)$, and both of them are the stationary points of the corresponding energy functional. However, their energy densities given by $w = \frac{1}{2}(1 \mp 2h_\perp d_z)$ are different. Therefore, we will only consider the spin-flop state $\mathbf{n} = (-1,0,0)$ with lower energy in our analysis. To examine the stability, we first introduce new fields

$$\begin{aligned}\Phi(x,y,t) &= -\frac{\pi}{2} + f(x,y,t),\\ \Theta(x,y,t) &= \frac{\pi}{2} + g(x,y,t),\end{aligned} \tag{B1}$$

where $f(x,y,t)$, $g(x,y,t)$ account for small fluctuations around the spin-flop state. Now, the actual parametrization of the staggered magnetization $\mathbf{n}$ given by Eq. (B1) is inserted in the complete Lagrangian of Eq. (4), which is applied for a magnetic field $\mathbf{h}$ given by Eq. (33) and expanded to quadratic order in f, g. If we further perform the usual Fourier transformation with frequency ω and wave vector $\mathbf{q} = (q_1,q_2)$, the corresponding linearized equations of motion can be solved analytically to yield the (squared) eigenfrequencies

$$\begin{aligned}\omega_\pm^2(\mathbf{q}) = q_1^2 + q_2^2 + h_\perp d_z + \tfrac{1}{2}\big(1 + h_z^2 + h_\perp^2\\ \pm\sqrt{\left(1 + h_z^2 - h_\perp^2\right)^2 + 4h_z^2h_\perp^2 + 16q_2^2}\big).\end{aligned} \tag{B2}$$

The above calculated magnon spectrum is strongly anisotropic. To examine the local stability of the spin-flop state, we note that the stability condition requires that $\omega_+^2 \geqslant 0$ and $\omega_-^2 \geqslant 0$ for each **q**. It is also clear that $\omega_+^2 \geqslant \omega_-^2$, and ω_-^2 is minimum for $q_1 = 0$. Therefore, we minimize ω_-^2 with respect to q_2 and then set $\omega_-^2 = 0$ to obtain

$$h_z^2 = 3 - h_\perp^2 - 2\sqrt{h_\perp^2 + 4h_\perp d_z}. \tag{B3}$$

The above-obtained line of local stability of the spin-flop state is displayed by the dashed line in the phase diagram of Fig. 4. Below the dashed line, the spin-flop state is locally unstable and can not exist. Note that Eq. (B3) applied for the special case $h_\perp = 0$ yields $h_z = \sqrt{3}$ ($H_z = 2.9$ T), which is just the upper critical field h_{c2} obtained in Ref. 24.

---

[*] Jaroslav.Chovan@umb.sk

[†] marder@mail.utexas.edu

[‡] papanico@physics.uoc.gr

[1] I. E. Dzyaloshinskii, Zh. Eksp. Teor. Fiz. **32**, 1547 (1957) [Sov. Phys.–JETP **5**, 1259 (1957)].

[2] T. Moriya, Phys. Rev. Lett. **4**, 228 (1960).

[3] H. Murakawa, Y. Onose, and Y. Tokura, Phys. Rev. Lett. **103**, 147201 (2009).

[4] S. Seki, X. Z. Yu, S. Ishiwata, and Y. Tokura, Science **336**, 198 (2012).

[5] S. Seki, S. Ishiwata, and Y. Tokura, Phys. Rev. B **86**, 060403(R) (2012).

[6] A. Bogdanov and D. Yablonski, Zh. Eksp. Teor. Fiz. **95**, 178 (1989) [Sov. Phys.–JETP **68**, 101 (1989)]; A. Bogdanov and A. Hubert, J. Magn. Magn. Mater. **138**, 255 (1994); U. K. Rößler, A. N. Bogdanov, and C. Pfleiderer, Nature (London) **442**, 797 (2006).

[7] A. Bogdanov and D. Yablonski, Zh. Eksp. Teor. Fiz. **96**, 253 (1989) [Sov. Phys.–JETP **69**, 142 (1989)]; A. Bogdanov and A. Shestakov, Phys. Solid State **40**, 1350 (1999).

[8] A. N. Bogdanov, U. K. Rößler, M. Wolf, and K.-H. S. Müller, Phys. Rev. B **66**, 214410 (2002).

[9] S. Mühlbauer, B. Binz, F. Jonietz, C. Pfleiderer, A. Rosch, A. Neubauer, R. Georgii, and P. Böni, Science **323**, 915 (2009).

[10] X. Z. Yu, Y. Onose, N. Kanazawa, J. H. Park, J. H. Han, Y. Matsui, N. Nagaosa, and Y. Tokura, Nature (London) **465**, 901 (2010).

[11] X. Z. Yu, N. Kanazawa, Y. Onose, K. Kimoto, W. Z. Zhang, S. Ishiwata, Y. Matsui, and Y. Tokura, Nat. Mater. **10**, 106 (2011).

[12] A. B. Borisov, J. I. Kishine, I. G. Bostrem, and A. S. Ovchinnikov, Phys. Rev. B **79**, 134436 (2009).

[13] F. Li, T. Nattermann, and V. L. Pokrovsky, Phys. Rev. Lett. **108**, 107203 (2012).

[14] V. V. Kiselev and A. A. Raskovalov, J. Exper. Theor. Phys. **116**, 272 (2013).

[15] A. Zheludev, G. Shirane, Y. Sasago, N. Koide, and K. Uchinokura, Phys. Rev. B **54**, 15163 (1996).

[16] A. Zheludev, S. Maslov, G. Shirane, Y. Sasago, N. Koide, and K. Uchinokura, Phys. Rev. B **57**, 2968 (1998).

[17] A. Zheludev, S. Maslov, G. Shirane, I. Tsukada, T. Masuda, K. Uchinokura, I. Zaliznyak, R. Erwin, and L. P. Regnault, Phys. Rev. B **59**, 11432 (1999).

[18] A. Zheludev, S. Maslov, G. Shirane, Y. Sasago, N. Koide, K. Uchinokura, D. A. Tennant, and S. E. Nagler, Phys. Rev. B **56**, 14006 (1997).

[19] A. Zheludev, S. Maslov, G. Shirane, Y. Sasago, N. Koide, and K. Uchinokura, Phys. Rev. Lett. **78**, 4857 (1997).

[20] I. E. Dzyaloshinskii, Zh. Eksp. Teor. Fiz. **47**, 992 (1964) [Sov. Phys.–JETP **20**, 665 (1965)].

[21] P. G. de Gennes, Solid State Commun. **6**, 163 (1968).

[22] R. B. Meyer, Appl. Phys. Lett. **14**, 208 (1969).

[23] P. G. de Gennes and J. Prost, *The Physics of Liquid Crystals* (Clarendon, Oxford, 1995).

[24] J. Chovan, N. Papanicolaou, and S. Komineas, Phys. Rev. B **65**, 064433 (2002).

[25] J. Chovan, Ph.D. thesis, P. J. Šafárik University, Košice, 2002.

[26] J. Chovan and N. Papanicolaou, *Frontiers in Magnetic Materials*, edited by A. N. Narlikar (Springer, Berlin, 2005), p. 347–384.

[27] J. Chovan and N. Papanicolaou, Ukr. J. Phys. **50**, 747 (2005), arXiv:cond-mat/0504262.

[28] S. Mühlbauer, S. N. Gvasaliya, E. Pomjakushina, and A. Zheludev, Phys. Rev. B **84**, 180406(R) (2011).

[29] S. Mühlbauer, S. N. Gvasaliya, E. Ressouche, E. Pomjakushina, and A. Zheludev, Phys. Rev. B **86**, 024417 (2012).

[30] T. A. Kaplan, Z. Phys. B **49**, 313 (1983); L. Shekhtman, O. Entin-Wohlman, and A. Aharony, Phys. Rev. Lett. **69**, 836 (1992); L. Shekhtman, A. Aharony, and O. Entin-Wohlman, Phys. Rev. B **47**, 174 (1993).

[31] M. D. Lumsden, B. C. Sales, D. Mandrus, S. E. Nagler, and J. R. Thompson, Phys. Rev. Lett. **86**, 159 (2001).